Spectrally wide acoustic frequency combs generated using oscillations of polydisperse gas bubble clusters in liquids

Bui Quoc Huy Nguyen and Ivan S. Maksymov[*]

Optical Sciences Centre, Swinburne University of Technology, Hawthorn, Victoria 3122, Australia

Sergey A. Suslov

Department of Mathematics, Swinburne University of Technology, Hawthorn, Victoria 3122, Australia

Acoustic frequency combs leverage unique properties of the optical frequency comb technology in high-precision measurements and innovative sensing in optically inaccessible environments such as under water, under ground, or inside living organisms. Because acoustic combs with wide spectra would be required for many of these applications but techniques of their generation have not yet been developed, here we propose an approach to the creation of spectrally wide acoustic combs using oscillations of polydisperse gas bubble clusters in liquids. By means of numerical simulations, we demonstrate that clusters consisting of bubbles with precisely controlled sizes can produce wide acoustic spectra composed of equally spaced coherent peaks. We show that under typical experimental conditions, bubble clusters remain stable over time, which is required for a reliable recording of comb signals. We also demonstrate that the spectral composition of combs can be tuned by adjusting the number and size of bubbles in a cluster.

I. INTRODUCTION

Frequency combs (FCs) are spectra containing equidistant coherent peaks. Although mostly optical FCs have found widespread practical and fundamental applications so far [1,2], in general, FCs can be generated using waves other than light. For example, a number of acoustic, phononic, and acousto-optical FC techniques have recently been introduced [3–13]. Among them, the acoustic frequency comb (AFC) techniques stand out because they hold the promise to enable ultrasensitive vibration detectors [14], phonon lasers [15,16], and quantum computers [17]. AFCs can also find applications in precision measurements in diverse physical, chemical, and biological systems in conditions, where using light—and hence optical FCs—poses technical and fundamental limitations. For example, this is the case in underwater distance measurements [9] and also in some biomedical imaging modalities [3,6,10].

In our previous work [13], we have theoretically and experimentally demonstrated the possibility of generating AFCs using oscillations of a cluster of gas bubbles in liquids [18–20]. We used low-pressure harmonic ultrasound signals with the frequency that is an order of magnitude higher than the natural frequency of the bubble cluster [19,21]. The interaction of ultrasound waves with an oscillating bubble at the natural frequency of a cluster results in the amplitude modulation of cluster's response and the appearance of sidebands around the harmonic and ultraharmonic peaks of the

driving ultrasound wave. We demonstrated that such sideband structures can be used as AFCs.

However, as with other AFC generation techniques [6,8], in our experiments the number of sideband peaks usable as an AFC is small. At present, this restriction presents numerous technological challenges that shape research efforts in the field of FCs [1,2]. For example, similarly to optical FCs, for many applications the AFC spectrum has to span over an octave of a bandwidth—that is, the highest frequency in the comb spectrum has to be at least twice the lowest frequency. Of course, the spectrum of an AFC can be extended using one of the techniques developed, for example, for broadening the spectra of optoelectronic FCs [22] such as supercontinuum generation using nonlinear optical effects. (Here, the adoption of optical techniques in the acoustic domain is possible because of the analogy between nonlinear optical processes in photonic devices and nonlinear acoustic processes in liquids containing gas bubbles [10].) Furthermore, our analysis reported in Ref. [13] demonstrates that the number of peaks in a bubble-generated AFC and their relative magnitude can be increased by simultaneously decreasing the frequency and increasing the pressure of the ultrasound wave driving bubble oscillations.

In the current paper, we suggest an alternative strategy for broadening spectra of AFCs generated using oscillations of gas bubbles. We theoretically investigate the use of polydisperse clusters consisting of mm-sized bubbles with equilibrium radii $R_{n0} = R_{10}/n$, where R_{10} is the equilibrium radius of the largest bubble in the cluster and $n = 1, 2, 3, \ldots$ is the number of bubbles in the cluster. Although clusters with other bubble size distributions could be used in the proposed approach, the specific ratio of equilibrium radii investigated in

_____
[*]imaksymov@swin.edu.au

this paper allows generating AFCs with a quasicontinuum of equally spaced peaks, which is convincingly demonstrated below by numerical simulations of clusters with $n = 4$ bubbles. In line with our previous experiments [13], in our analysis we consider low-pressure ultrasound waves (up to 10 kPa). We show that the ultrasound frequency can be chosen in a wide spectral range above the natural oscillation frequency of individual bubbles in the cluster. Our calculations demonstrate that these relaxed technical specifications can greatly facilitate the generation and recording of stable AFC signals. This is because at low pressure, insonification bubble clusters exhibit regular behavior until the bubble dynamics becomes affected by their aggregation [13]. Moreover, formation of a bubble cluster with mm-range equilibrium radii of about $2/n$ mm is technologically straightforward and can be accomplished using only a simple bubble generator equipped with a customised air diffuser [13].

It is noteworthy that stable gas bubble clusters called bubble grapes have been previously generated [23–26] using low-pressure ultrasound waves. However, as discussed in Sec. II, bubble grapes are formed when the sign of the secondary Bjerknes force is reversed and the corresponding equilibrium state becomes stable [27]. In contrast, we propose to generate AFCs in a regime where the bubbles attract each other but the magnitude of the secondary Bjerknes force is very small due to the disparate natural bubble frequencies and the frequency of the driving ultrasound wave. As a result, the interbubble distance and the overall arrangement of bubbles within a cluster appear to be sufficiently stable for the observation of well-pronounced AFC spectra without applying any additional cluster stabilization procedures.

II. BACKGROUND THEORY

The accepted model of nonlinear oscillations of a single gas bubble that does not undergo translational motion is given by the Keller-Miksis (KM) equation [28] that takes into account the decay of bubble oscillations due to viscous dissipation and fluid compressibility. However, when the focus is on mm-sized gas bubbles oscillating at 20–100 kHz frequencies in water being driven by low-pressure ultrasound waves (with the amplitude of up to 10 kPa), the terms in the KM equation accounting for fluid compressibility become negligible [13]. Thus, the KM equation effectively reduces to the classical Rayleigh-Plesset (RP) equation [29,30] that we use as the base model in what follows.

As with a single bubble, the RP equation for a cluster consisting of N bubbles not undergoing translational motion can be obtained by removing the acoustic loss terms from the generalized KM equation for a bubble cluster [31,32]:

$$R_n \frac{d^2 R_n}{dt^2} + \frac{3}{2}\left(\frac{dR_n}{dt}\right)^2 = \frac{1}{\rho}\left(P\left(R_n, \frac{dR_n}{dt}\right) - P_\infty(t)\right) - P_{sn}, \quad (1)$$

where

$$P_n\left(R_n, \frac{dR_n}{dt}\right) = \left(P_0 - P_v + \frac{2\sigma}{R_{n0}}\right)\left(\frac{R_{n0}}{R_n}\right)^{3\kappa} - \frac{4\mu}{R_n}\frac{dR_n}{dt} - \frac{2\sigma}{R_n}. \quad (2)$$

The term accounting for the pressure acting on of the nth bubble due to scattering of the incoming pressure wave by the neighboring bubbles in a cluster is given by

$$P_{sn} = \sum_{l=1, l\neq n}^{N} \frac{1}{d_{nl}}\left(R_l^2 \frac{d^2 R_l}{dt^2} + 2R_l\left(\frac{dR_l}{dt}\right)^2\right), \quad (3)$$

where d_{nl} is the interbubble distance and N is the total number of bubbles in the cluster [31] (more comprehensive models of bubble interaction in a cluster are available in the literature, e.g., Ref. [33], but the above simple treatment will suffice in the context of the current study). The expression $P_\infty(t) = P_0 - P_v + \alpha \sin(\omega^* t)$ with the angular frequency $\omega^* = 2\pi f$ represents the periodically varied pressure in the liquid far from the bubble. Parameters R_{n0}, $R_n(t)$, μ, ρ, κ, σ, α, and f denote the equilibrium and instantaneous radii of the nth bubble in the cluster, the dynamic viscosity and the density of the liquid, the polytropic exponent of a gas entrapped in the bubble, the surface tension of a gas-liquid interface, and the amplitude and the frequency of a driving ultrasound wave. Diffusion of the gas through the bubble surface is neglected.

When bubble oscillations are not affected by fluid compressibility, which is the case in this work, the acoustic power scattered by the nth bubble in the cluster in the far-field zone is [18]

$$P_{\text{scat}}(R_n, t) = \frac{\rho R_n}{h}\left(R_n \ddot{R}_n + 2\dot{R}_n^2\right), \quad (4)$$

where h is much larger than the spatial extent of the cluster.

Interactions of gas bubbles, including their radial oscillations and translational motion driven by an acoustic pressure field has been a subject of intensive research (see, e.g., Refs. [27,31,32,34–48]; for a review, see Ref. [49]). Most of these works are based on the accepted models of spherical gas bubble oscillations [Eqs. (1)–(3)] and account for the action of Bjerknes forces [50]. The primary Bjerknes force F_{pB} is caused by the acoustic pressure field [50,51] while the secondary Bjerknes force F_{sB} arises between two and more bubbles in the same pressure field [49]. The secondary Bjerknes force between two gas bubbles is repulsive when the driving frequency lies between the natural frequencies of the bubbles, otherwise it is attractive [49]. This theoretical prediction was confirmed experimentally [52,53].

However, several important experimental observations cannot be explained using Bjerknes theory. These include the formation of stable bubble grape clusters [23,25] and self-organization effects in bubble-liquid mixtures [54] that explain acoustic streaming phenomena [40,55] and underpin some techniques of bubble manipulation [47].

Kobelev *et al.* [23] were the first to report the formation of bubble grapes as a byproduct of their experiment targeting the attenuation of sound in liquids containing gas bubbles. They demonstrated that nonlinear oscillations of gas bubbles

cannot be responsible for the observed effect. The original Bjerknes force theory [49–51] based on the linear oscillations of gas bubbles is unable to explain this phenomenon either since it applies only to gas bubbles separated by distances that are much larger than the bubble radii and because it only predicts whether the bubbles attract or repulse depending on their natural frequencies. Thus, the only plausible explanation of the formation of bubble grapes could be a reversal in the secondary Bjerknes force from attractive to repulsive.

One attempt to theoretically explain the formation of bubble grapes was made by Nemtsov [34]. However, his model did not account for wave scattering by bubbles [49]. Zabolotskaya [27] developed a model explaining the sign reversal of the secondary Bjerknes force. Oguz and Prosperetti [56] theoretically demonstrated the possibility of sign reversal of the secondary Bjerknes force in the case of nonlinear bubble oscillations driven by high-pressure acoustic waves. However, the result presented in their work cannot explain linear processes underlying the formation of bubble grapes. Subsequently, Zabolotskaya's theory was extended by Doinikov and Zavtrak [49] and used to explain [25] an intriguing observation of stable bubble structures in an experiment involving strongly forced mm-sized gas bubbles oscillating in low gravity conditions [24]. An alternative interpretation of the sign reversal of the secondary Bjerknes force was proposed in Ref. [57].

However, although the experimental conditions in our work reported in Ref. [13] indeed resemble those required for the formation of bubble grapes, the bubble clusters we observed form due to a different mechanism that does not involve the sign reversal of Bjerknes force. This is because we use mm-size bubbles with the natural frequencies of 1–3 kHz but drive their oscillations with a low-pressure high-kHz-range ultrasound. As a result, although the aggregation and eventual coalescence of bubble are inevitable in our experiments, they occur on a timescale of several seconds and hence are mostly inconsequential for the generation of AFCs.

III. INTERACTION BETWEEN TWO GAS BUBBLES

The interaction dynamics of gas bubbles oscillating in liquids is very complex because the cluster geometry varies from experiment to experiment and with time. Therefore, many theoretical works consider a system of just two interacting bubbles surrounded by an idealized liquid. This simplification allows reducing the complexity of the model while accounting for the essential physics of bubble interaction.

A. Analysis of the RP equation for two interacting gas bubbles

To identify the main characteristics of nonlinear oscillations of interacting gas bubbles relevant to the generation of AFCs, we conduct an asymptotic analysis of Eq. (1), extending our previous model of nonlinear oscillations of a single gas bubble [13].

We start with rewriting Eq. (1) in the nondimensional form using the equilibrium radius of the largest bubble in the cluster, R_{10}, and $1/\omega^*$ as the length scale and timescale, respectively, to introduce the nondimensional quantities $r_n = R_n(t)/R_{10}$, $r_l = R_l(t)/R_{10}$, and $\tau^* = \omega^* t$ [32]. Substituting

these into Eq. (1), we obtain

$$r_n r_n'' + \frac{3}{2} r_n'^2 = \left(\mathcal{M} + \frac{\mathcal{W}}{\mathcal{Q}_n} \right) \left(\frac{\mathcal{Q}_n}{r_n} \right)^{\mathcal{K}} - \frac{\mathcal{W}}{r_n} - \mathcal{R} \frac{r_n'}{r_n} - \mathcal{M}$$

$$- \mathcal{M}_e \sin \tau^* - \sum_{\substack{l=1 \\ l \neq n}}^{N} \zeta_{nl} \left(r_l^2 r_l'' + 2 r_l r_l'^2 \right), \quad (5)$$

where $\mathcal{R} = \dfrac{4\mu}{\rho \omega^* R_{10}^2}$, $\mathcal{W} = \dfrac{2\sigma}{\rho \omega^{*2} R_{10}^3}$, $\mathcal{M} = \dfrac{P_0 - P_v}{\rho \omega^{*2} R_{10}^2}$, $\mathcal{M}_e = \dfrac{\alpha}{\rho \omega^{*2} R_{10}^2}$, $\zeta_{nl} = \dfrac{R_{10}}{d_{nl}}$, $\mathcal{K} = 3\kappa$, and $\mathcal{Q}_n = \dfrac{R_{n0}}{R_{10}}$. Parameter $\mathcal{M}$ characterizes the ratio of a bubble's natural and forced oscillation frequencies, $\mathcal{W}$ and $\mathcal{R}$ can be treated as inverse Weber and Reynolds numbers, representing the surface tension and viscous dissipation effects, respectively, and $\mathcal{M}_e$ is the measure of the ultrasound forcing [58]. Parameters ζ_{nl} and $\mathcal{Q}_n$ are the inverse of the distance between the bubble centers and the bubble radius relative to that of the largest bubble in the cluster, respectively [32], and primes denote differentiation with respect to t. As discussed in Refs. [13,58], $\mathcal{K} = 4$ for bubbles of sizes relevant to the AFC context and for the fluid parameters, ultrasound pressure and frequency given in Sec. IV the maximum values of other parameters do not exceed $\mathcal{M} = 9.7 \times 10^{-4}$, $\mathcal{W} = 7.4 \times 10^{-7}$, $\mathcal{R} = 6.5 \times 10^{-6}$, and $\mathcal{M}_e = 9.9 \times 10^{-5}$. Therefore, the effects of water viscosity and surface tension on bubble oscillations are negligible and we set $\mathcal{R} = \mathcal{W} = 0$ in what follows. Thus, ultrasonically forced bubble oscillations can be assumed perfectly periodic when the driving frequency is much higher than any of the natural frequencies of the individual bubbles in the cluster (i.e., no resonances arises). This warrants using a method similar to that in Ref. [13].

We consider a cluster consisting of two gas bubbles with the nondimensional equilibrium radii $r_{n0} = \mathcal{Q}_n$, $n = 1, 2$ ($\mathcal{Q}_1 \equiv 1$). Following Refs. [13,59], we look for the asymptotic solutions of Eq. (5) in the form

$$r_n = \mathcal{Q}_n + \epsilon r_{n1}(\tau) + \epsilon^2 r_{n2}(\tau) + \cdots, \quad n = 1, 2, \quad (6)$$

where $0 < \epsilon \ll 1$ is a parameter characterizing the amplitude of bubble oscillations used to distinguish between various terms in the asymptotic series and $\tau = \omega \tau^* = \omega \omega^* t$. At the first order of ϵ, we obtain

$$\ddot{r}_{11} + \frac{\mathcal{K}\mathcal{M}}{\mathcal{Q}_1^2 \omega^2} r_{11} + \frac{\mathcal{Q}_2^2}{\mathcal{Q}_1} \zeta_{12} \ddot{r}_{21} = \frac{p}{\mathcal{Q}_1} \sin(\Omega\tau), \quad (7)$$

$$\ddot{r}_{21} + \frac{\mathcal{K}\mathcal{M}}{\mathcal{Q}_2^2 \omega^2} r_{21} + \frac{\mathcal{Q}_1^2}{\mathcal{Q}_2} \zeta_{12} \ddot{r}_{11} = \frac{p}{\mathcal{Q}_2} \sin(\Omega\tau), \quad (8)$$

where overdots denote differentiation with respect to τ and we write $(\mathcal{M}_e/\omega^2) \sin \tau^* \equiv -\epsilon p \sin(\Omega\tau)$ and introduce $\Omega \equiv 1/\omega \gg 1$. For convenience we also choose $\omega^2 = \mathcal{K}\mathcal{M}$, where $\mathcal{K}\mathcal{M}$ is Minnaert frequency [13,21] of the largest bubble in the cluster. Finally, we obtain

$$\ddot{r}_{11} + r_{11} + \mathcal{Q}_2^2 \zeta_{12} \ddot{r}_{21} = p \sin(\Omega\tau), \quad (9)$$

$$\ddot{r}_{21} + \frac{1}{\mathcal{Q}_2^2} r_{21} + \frac{\zeta_{12}}{\mathcal{Q}_2} \ddot{r}_{11} = \frac{p}{\mathcal{Q}_2} \sin(\Omega\tau). \quad (10)$$

At $O(\epsilon^2)$, equations then become

$$\ddot{r}_{12} + r_{12} + \mathcal{Q}_2^2 \zeta_{12} \ddot{r}_{22} = \frac{\mathcal{K}+1}{2} r_{11}^2 - \frac{3}{2} \dot{r}_{11}^2 - r_{11} \ddot{r}_{11}$$
$$- 2\mathcal{Q}_2 \zeta_{12} (\dot{r}_{21}^2 + r_{21} \ddot{r}_{21}), \quad (11)$$

$$\ddot{r}_{22} + \frac{1}{\mathcal{Q}_2^2} r_{22} + \frac{\zeta_{12}}{\mathcal{Q}_2} \ddot{r}_{12} = \frac{\mathcal{K}+1}{\mathcal{Q}_2^2} r_{21}^2 - \frac{3}{2\mathcal{Q}_2} \dot{r}_{21}^2 - \frac{1}{\mathcal{Q}_2} r_{21} \ddot{r}_{21}$$
$$- 2\frac{\zeta_{12}}{\mathcal{Q}_2} (\dot{r}_{11}^2 + r_{11} \ddot{r}_{11}). \quad (12)$$

Similar to Ref. [13], we write the random initial conditions as $r_1(0) = 1 + \epsilon a$, $r_2(0) = \mathcal{Q}_2 + \epsilon b$, $\dot{r}_1(0) = \epsilon c$, and $\dot{r}_2(0) = \epsilon d$ that results in

$$r_{11}(0) = a, \ r_{21}(0) = b, \ \dot{r}_{11}(0) = c, \ \dot{r}_{21}(0) = d. \quad (13)$$

Subsequently, we obtain the leading order solutions

$$r_{11}(\tau) = C_1 \cos(\omega_1' \tau + \phi_1) + C_2 \cos(\omega_2' \tau + \phi_2)$$
$$+ B_1 \sin \Omega \tau, \quad (14)$$

$$r_{21}(\tau) = C_3 \cos(\omega_1' \tau + \phi_1) + C_4 \cos(\omega_2' \tau + \phi_2)$$
$$+ B_2 \sin \Omega \tau, \quad (15)$$

where $\omega_{1,2}' = \dfrac{\sqrt{2}}{\sqrt{\mathcal{Q}_2^2 + 1 \pm \sqrt{(\mathcal{Q}_2^2 - 1)^2 + 4\mathcal{Q}_2^3 \zeta_{12}^2}}}$. These frequencies depend on the inverse of the interbubble distance ζ_{12}, which is a well-established fact [27,49,60]. Considering a particular case of $\mathcal{Q}_2 = \frac{1}{2}$, as expected, for noninteracting distant bubbles with $\zeta_{12} \to 0$ we obtain $\omega_1' \to \omega_{10}' = 1$ and $\omega_2' \to \omega_{20}' = 2$. In general, the leading order bubble response will always contain three distinct frequencies: two bubbles' natural frequencies $\omega_{1,2}'$ and the driving ultrasound frequency Ω.

Coefficients C_{1-4} and phase shifts $\phi_{1,2}$ in Eqs. (14) and (15) depend on ζ_{12}, Ω, and p. As shown in Ref. [13], their exact expressions can be obtained for arbitrary initial conditions (13). However, the resulting expressions are too long to be given here explicitly and we only discuss the physical conclusions that follow from them. Specifically, these coefficients demonstrate that the spectra of both bubbles contain frequencies Ω and $\omega_{1,2}'$. The magnitude of the ω_1' peak is greater than that of ω_2' in the spectrum of bubble 1 and vice versa. In the spectra of both bubbles, the amplitude of the peak corresponding to the frequency of a neighboring bubble decreases with the distance between them and vanishes when the interaction between them becomes negligible.

Analysis of Eqs. (10) and (12) can be performed following the procedure outlined in Ref. [13]. However, here we do not pursue this any further since, for the purposes of the current paper, it suffices to note that the right-hand sides of these equations contain quadratic terms involving r_{11} and r_{12} and their derivatives. Therefore, in addition to the harmonic components with frequencies $\omega_{1,2}'$ solutions of Eqs. (10) and (12) will include steady and periodic terms with frequencies equal to all possible pairwise sums and differences of $\omega_{1,2}'$ and Ω: $\omega_{1,2}' \pm \omega_{2,1}'$, $\Omega \pm \omega_{1,2}'$, $2\omega_{1,2}'$, and 2Ω.

B. Bjerknes force between two oscillating bubbles

The asymptotic analysis in Sec. III A shows that, when the bubble oscillations are driven by a low-pressure ultrasound wave, the magnitude of any nonlinear effect is proportional to $\mathcal{M}_e^2 \sim 9.8 \times 10^{-9}$ (as per experimental conditions in Ref. [13]). Hence, the nonlinearity is neglected in this section.

Two physically equivalent dimensional expressions accounting for a sign reversal of Bjerknes force arising between two oscillating gas bubbles separated by a distance that is much larger than bubble radii were derived previously in Refs. [27,49]. From the expression given by Eq. (2.5) in Ref. [49], we obtain the leading term of the nondimensional secondary Bjerknes force (scaled with $\rho \omega^{*2} R_{10}^4$),

$$F_{sB}' = -4\pi \zeta_{12}^2 \mathcal{Q}_2^2 \omega^2 \epsilon^2 \langle r_{11} \ddot{r}_{21} \rangle, \quad (16)$$

where the angle brackets denote time averaging. Substituting expressions (14) and (15) into Eq. (16), taking into account that $|\omega_1' - \omega_2'| \sim 1$, we obtain

$$F_{sB}' = 2\pi \zeta_{12}^2 \mathcal{Q}_2^2 \omega^2 \epsilon^2 \left(B_1 B_2 \Omega^2 + C_1 C_3 {\omega_1'}^2 + C_2 C_4 {\omega_2'}^2 \right).$$

Evaluating coefficients $B_{1,2}$ and C_{1-4} in the limit $\zeta_{12} \to 0$ finally leads to

$$F_{sB}' = 4\pi \zeta_{12}^2 \mathcal{Q}_2^2 \mathcal{M}_e^2 \frac{\Omega^8}{(\Omega - 1)^2 (\Omega + 1)^2}. \quad (17)$$

Here we focus on a particular bubble oscillation regime [13] characterized by $\Omega \gg 1$. In this case,

$$F_{sB}' \to 4\pi \zeta_{12}^2 \mathcal{Q}_2^2 \mathcal{M}_e^2 \Omega^4 = 4\pi \zeta_{12}^2 \mathcal{Q}_2^2 \frac{\mathcal{M}_e^2}{\mathcal{K}^2 \mathcal{M}^2}. \quad (18)$$

By its definition, $Q_2 < 1$ and in the reference experiment [13] $\mathcal{M}_e / (\mathcal{K}\mathcal{M}) \sim 0.025$ and $\zeta_{12}^2 \lesssim 0.04$. Therefore, we conclude that the secondary Bjerknes force is small at the typical driving frequencies used in the generation of bubble-based AFCs away from bubble resonances. This provides an opportunity for measuring the acoustic bubble response and recording the resulting signals for AFC applications before bubble oscillations become affected by their aggregation. Our calculations, using a more rigorous model of a translational motion, the results of which are presented in Sec. IV, provide convincing arguments in favor of this.

C. Dynamics of multibubble clusters with translational motion

It has been shown in Ref. [61] that Eq. (1) can be extended to include the effect of a translational bubble motion. The resulting system of differential equations reads

$$R_n \ddot{R}_n + \frac{3}{2} \dot{R}_n^2 - \frac{P_n}{\rho}$$
$$= \frac{\dot{\mathbf{p}}_n}{4} - \sum_{\substack{l=1 \\ l \neq n}}^{N} \left\{ \frac{R_l^2 \ddot{R}_l + 2R_l \dot{R}_l^2}{d_{nl}} \right.$$
$$\left. + \frac{R_l^2}{2d_{nl}^3} (\mathbf{p}_n - \mathbf{p}_l) \cdot (R_l \ddot{\mathbf{p}}_l + \dot{R}_l \dot{\mathbf{p}}_n + 5\dot{R}_l \dot{\mathbf{p}}_l) \right.$$

$$- \frac{R_l^3}{4d_{nl}^3} \left[\dot{\mathbf{p}}_l \cdot (\dot{\mathbf{p}}_n + 2\dot{\mathbf{p}}_l) + \frac{3}{d_{nl}^2} [\dot{\mathbf{p}}_l \cdot (\mathbf{p}_l - \mathbf{p}_n)] \right.$$

$$\left. \times [(\mathbf{p}_n - \mathbf{p}_l) \cdot (\dot{\mathbf{p}}_n + 2\dot{\mathbf{p}}_l)] \right] \bigg\}, \qquad (19)$$

$$\frac{1}{3} R_n \ddot{\mathbf{p}}_n + \dot{R}_n \dot{\mathbf{p}}_n$$

$$= \frac{\mathbf{F}_n}{2\pi \rho R_n^2} + \sum_{\substack{l=1 \\ l \neq n}}^{N} \left\{ \frac{(\mathbf{p}_n - \mathbf{p}_l) B_1}{d_{nl}^3} - \frac{R_l^2}{2d_{nl}^3} [R_n R_l \ddot{\mathbf{p}}_l + B_2 \dot{\mathbf{p}}_l] \right.$$

$$\left. + \frac{3R_l^2}{2d_{nl}^5} (\mathbf{p}_n - \mathbf{p}_l) \langle (\mathbf{p}_n - \mathbf{p}_l) \cdot [R_n R_l \ddot{\mathbf{p}}_l + B_2 \dot{\mathbf{p}}_l] \rangle \right\}, \quad (20)$$

where overdots denote differentiation with respect to time, $B_1 = R_n R_l^2 \ddot{R}_l + 2R_n R_l \dot{R}_l^2 + \dot{R}_n \dot{R}_l R_l^2$, $B_2 = \dot{R}_n R_l + 5R_n \dot{R}_l$, $\mathbf{p}_{l,n}$ are the position vectors of the lth and nth bubble centers and $\mathbf{F}_n$ denotes the external force acting on the nth bubble.

Equation (19) describes the radial oscillations of the nth bubble in the cluster and Eq. (20) governs its translational motion. In these equations, similarly to Eqs. (1) and (2), the pressure P_n is defined as

$$P_n(R, \dot{R}) = \left(P_0 - P_v + \frac{2\sigma}{R_{n0}} \right) \left(\frac{R_{n0}}{R_n} \right)^{3\kappa} - \frac{4\mu \dot{R}_n}{R_n} - \frac{2\sigma}{R_n}$$
$$- P_0 - P_v - P_{\text{ex}}(\mathbf{p}_n), \qquad (21)$$

where $P_{\text{ex}}(\mathbf{p}_n)$ is the pressure of the driving ultrasound wave in the center of the nth bubble. The external forces $\mathbf{F}_n$ are the sum of the primary Bjerknes force

$$\mathbf{F}_{nB} = -\frac{4\pi}{3} R_n^3 \nabla P_{\text{ex}}(\mathbf{p}_n) \qquad (22)$$

and the force exerted on the bubble by the surrounding fluid (see Ref. [62], Chap. 8, Sec. 82 [63]), which in the case of the oscillating bubble is given by [61]

$$\mathbf{F}_{nL} = -12\pi \mu R_n \left(\dot{\mathbf{p}}_n - \mathbf{v}_{\text{ex}}(\mathbf{p}_n) - \sum_{\substack{l=1 \\ l \neq n}}^{N} \mathbf{v}_{ln} \right), \quad (23)$$

where $\mathbf{v}_{\text{ex}}(\mathbf{p}_n)$ is the liquid velocity forced by the driving pressure field in the center of the nth bubble. The fluid velocity generated by the lth bubble in the center of the nth bubble is given by

$$\mathbf{v}_{nl} = \frac{R_l^2 \dot{R}_l (\mathbf{p}_n - \mathbf{p}_l)}{d_{nl}^3}$$
$$+ \frac{R_l^3}{2d_{nl}^3} \left\{ \frac{3(\mathbf{p}_n - \mathbf{p}_l)}{d_{nl}^2} [\dot{\mathbf{p}}_l \cdot (\mathbf{p}_n - \mathbf{p}_l)] - \dot{\mathbf{p}}_l \right\}. \qquad (24)$$

Note that although the model Eqs. (19)–(24) were derived for the case of microscopic gas bubbles driven by high-pressure ultrasound fields [61], all its equations remain valid for mm-size bubbles [62].

IV. NUMERICAL RESULTS

Computations have been performed for the following fluid parameters corresponding to water at $20\,^\circ$C: $\mu = $

10^{-3} kg m/s, $\sigma = 7.25 \times 10^{-2}$ N/m, $\rho = 10^3$ kg/m^3, and $P_v = 2330$ Pa. We take the air pressure in a stationary bubble to be $P_0 = 10^5$ Pa and the polytropic exponent of air to be $\kappa = 4/3$. The duration of a typical simulation is 2000 oscillation periods of the driving ultrasound wave.

The system of equations (19) and (20) is solved numerically using a fixed-step fourth-order Runge-Kutta method implemented in a customised subroutine rk4 [64] ported from Pascal to Oberon-07 programming language. The accuracy of this subroutine was tested by solving Eq. (1) for a single gas bubble and comparing the result with a solution obtained using a standard adaptive-step subroutine ode45 in the Octave software. While essentially the same results were obtained using both subroutines, Oberon-07-based computations are an order of magnitude faster and thus are preferred for modeling multibubble clusters.

We analyze an acoustic response of four clusters that consist of two, three, and four bubbles with the equilibrium radii $R_{n0} = R_{10}/n$, where n is the number of the bubbles and $R_{10} = 1.95$ mm is the typical bubble radius used in Ref. [13]. The frequency of the driving sinusoidal ultrasound wave propagating in the positive z direction is 26 kHz and its peak pressure is 10 kPa. The coordinates of the centers of the bubbles are $(x, y, z) = (-2.5R_{10}, 0, -2.5R_{10})$, $(2.5R_{10}, 0, 2.5R_{10})$, $(0, 4.33R_{10}, 0.2R_{10})$, and $(0, -4.33R_{10}, -0.1R_{10})$. This specific configuration resembles a typical bubble cluster arrangement observed in our experiments [13]. Results qualitatively similar to those presented below were obtained using other cluster configurations with the same equilibrium radii of the bubbles and distances between them.

Figure 1 shows the calculated spectra of the bubble clusters (shown by color-filled regions). The number of rows in each column corresponds to the total number of bubbles in the cluster. Each column shows the spectrum of the pressure scattered by an individual bubble within the cluster [calculated using Eq. (4) for each bubble]. Analyzing panels within the same row from left to right, we observe changes in the AFC peak structure caused by the addition of smaller bubbles to the cluster. For example, the four panels in the top row considered from left to right demonstrate that the number of equidistant peaks in the AFC spectrum produced by the largest bubble increases when smaller bubbles are added. This is because bubbles within a cluster are affected by pressure waves scattered by their neighbors and thus their spectra include additional frequency peaks compared to the spectra of isolated noninteracting stationary bubbles of the same equilibrium radii calculated using Eq. (1) and shown by the dashed lines. Similarly, panels in the second row show the evolution of the AFC spectrum of the second largest bubble in the cluster, and so on. In all cases, the spectra exhibit the key features pertinent to the generation of AFCs: the spectrum of the acoustic response of each bubble consists of a series of well-defined equally spaced peaks.

For a two-bubble cluster, these observations agree with predictions of our asymptotic analysis in Sec. III A. Indeed, in the leftmost column in Fig. 1, we can identify (counting from from left to right) a pair of peaks at the natural frequencies of the first and second bubbles and two other at the second harmonics of these frequencies. In each pair, the peak
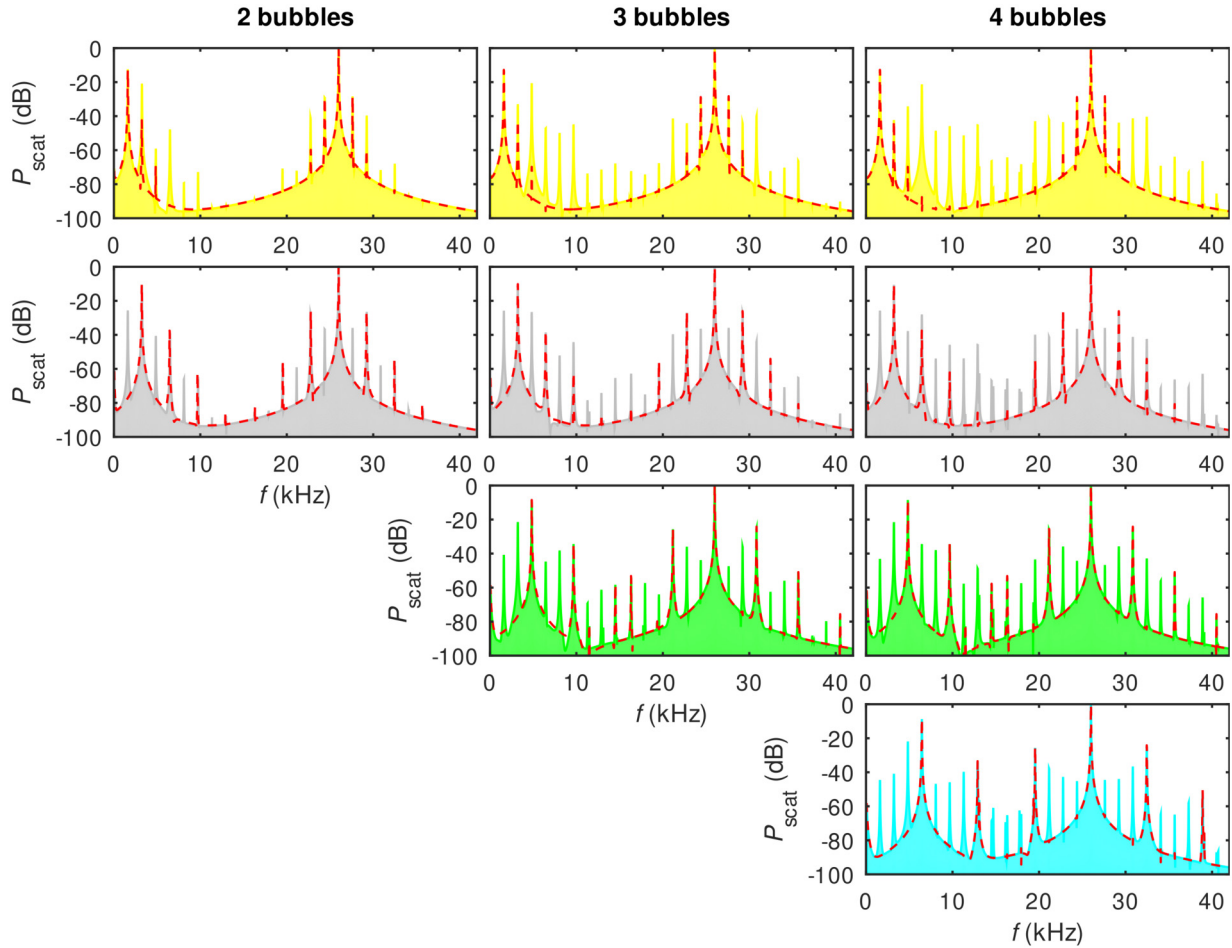
FIG. 1. Columns, from left to right, show the AFC spectra produced by the individual bubbles within the clusters consisting of two, three, and four gas bubbles with the equilibrium radii $R_{n0} = 1.95/n$ mm, where n is the index number of the bubble in the cluster. The number of panels in each column corresponds to the total number of bubbles in the cluster. The red dashed lines in each panel show the spectra of individual non-interacting stationary bubbles with identical equilibrium radii. Computational parameters are given in the main text.

corresponding to oscillations at the natural frequency of the first (second) bubble has a larger magnitude than that induced by the second (first) bubble in the cluster. All these peaks give rise to the sideband structure around the peak at the forcing frequency (26 kHz), the highest peak in both spectra (and also at its ultraharmonic at 42 kHz that is not shown in Fig. 1). The relative magnitude of the sideband peaks follows the pattern of the peaks originating from oscillations at the natural frequencies of the bubbles. The results of our numerical simulation also indicate the presence of the third and fourth harmonics of the natural frequencies in the spectrum of the cluster response above the noise level. Capturing them analytically is straightforward but would require retaining cubic and quartic terms in ϵ in expansions (6), thus leading to very long algebraic expressions. For this reason, we do not present them here.

A similar but more complex picture is observed in the cases of three and four bubbles, where the triplets and quadruples of the peaks corresponding to the natural frequencies of the bubbles and their harmonics can be identified. Furthermore, these peak ensembles generate the sideband peak structures around the forcing frequency, thereby forming a quasicontinuum of equally spaced peaks, which is important for AFC applica-

tions. However, a detailed analysis of the origin of individual peaks in such a quasicontinuous spectrum in large clusters, while straightforward, is somewhat tedious and here we limit ourselves to discussing the spectra of clusters consisting of up to four bubbles.

Of course, the magnitudes of the peaks originating from the bubbles of different sizes are different. However, whereas generating peaks of the same magnitude would be advantageous for certain AFCs applications, having peaks of different magnitudes is, in general, inconsequential as long as they are detectable and their frequencies are stable (see Ref. [13] for a comprehensive discussion of this technical aspect).

It follows from this discussion that accounting for the translational motion of bubbles does not noticeably alter computational results. This fact was confirmed by comparing the spectra in Fig. 1 with those calculated for the case of motionless bubbles (not shown) and establishing that all results are virtually indistinguishable within the limits of computational accuracy. We also note that the spectral line positions and shapes corresponding to bubbles undergoing translational motion and interacting with their neighbors are almost identical to those of isolated noninteracting stationary gas bubbles (compare the color-filled spectra with the spectra shown by
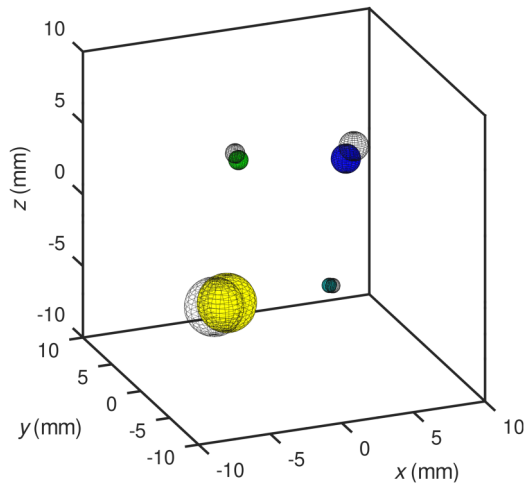
FIG. 2. Initial arrangement of bubbles in the four-bubble cluster (the transparent spheres) and the position of the same bubbles after 2000 periods of oscillations of the driving ultrasound wave (colored spheres).

the red dashed lines in each panel in Fig. 1). This means that bubble translation does not affect their natural frequency within the considered computational time.

In support of this conclusion, in Fig. 2 we compare the initial spatial bubble positions in a four-bubble cluster investigated above with the positions of the same bubbles after 2000 periods of the driving ultrasound wave. In agreement with the results of the analysis presented in Sec. III B, we observe that bubble attraction is weak so even after 2000 periods of oscillations the distance between them remains sufficiently large for the cluster to generate a usable AFC spectrum (and for the model to remain validity).

In highly populated clusters, the probability of bubble collision and coalescence increases, which may lead to an undesirable random change of the cluster frequency spectrum. To assess the scalability of the proposed bubble-based AFC

generation, we performed a series of calculations with $n > 4$ randomly located bubbles with sizes $R_{n0} = R_{10}/n$, where the integer parameter n was randomly chosen from the range $[1 \dots 5]$. In all such computational tests, we observed that, provided that the initial interbubble distance was larger than the equilibrium bubble size, the bubble displacement over the first 2000 periods of the driving ultrasound wave remained small, see Fig. 3, where two representative eight-bubble arrangements used in our computations are shown. Therefore, it is demonstrated that, given that care is taken to create an initial cluster with well-separated bubbles, a stable bubble oscillation spectrum can be safely expected to exist over the time interval required for a reliable AFC generation.

V. CONCLUSIONS

We have proposed an approach to the generation of spectrally wide AFCs using oscillations of polydisperse gas bubble clusters in liquids. The plausibility of such an approach has been demonstrated via theoretical analysis and numerical simulation. In the model used in computations, we excite a bubble cluster with a low-pressure ultrasound wave at a frequency that is higher than the natural frequency of any bubble in the cluster. Bubbles within a cluster interact with each other and their acoustic spectra are affected by their neighbors. We choose the bubble sizes in such a way that their natural frequencies become integer multiples of the natural frequency of the largest bubble in the cluster. Because of that, the spectra of individual bubbles contain multiple peaks, each of which can be unambiguously associated with the specific bubble within the cluster.

In agreement with the analysis and experimental observations reported in our previous publication [13], the interference of bubble responses at their natural frequencies with the driving ultrasound wave results in the amplitude modulation of the latter and in the appearance of equally spaced sideband peaks in the spectrum. Moreover, the combination of sidebands and the ensemble of peaks originating directly from the oscillations at the natural bubble frequencies results
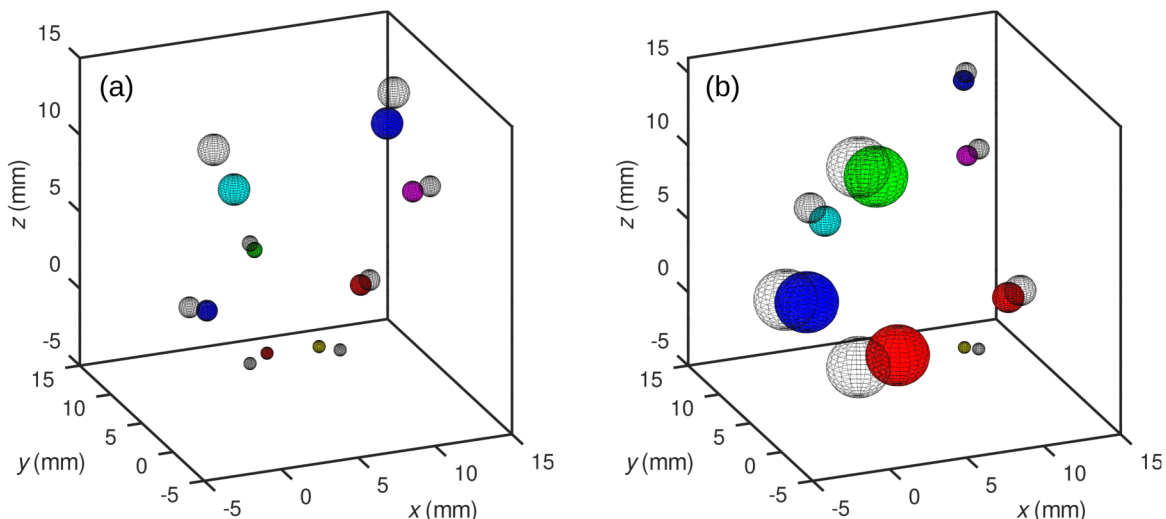

FIG. 3. Initial arrangement (described in the main text) in two representative eight-bubble clusters (the transparent spheres) and the position of the same bubbles after 2000 periods of oscillations of the driving ultrasound wave (colored spheres).

in a quasicontinuum of equally spaced peaks. Its spectral composition depends on bubble radii and the frequency of a driving ultrasound wave. Therefore, it can be tuned by changing either of these parameters. In particular, because mm-sized gas bubbles are required to generate AFCs discussed in this paper, a practical realization of the proposed approach is technically straightforward. Indeed, a simple customized bubble generator consisting of a standard air pump and a diffuser made of a suitable porous material [13] would suffice to produce bubble clusters with the configuration investigated in this paper. We have also demonstrated that the attraction and potential coalescence of oscillating bubbles due to the action of the secondary Bjerknes force do not affect the generation of the AFC because coalescence occurs at a timescale that is much larger than the time needed for a reliable recording of AFC signals. Our results are also expected to apply to smaller gas bubbles driven by ultrasound waves in high kHz and MHz frequency ranges, which paves the way for the generation of AFCs suitable for a wide range of technologically important applications.

Finally, we note that there exist several techniques suitable for separating individual bubble contributions to the overall pressure signal emitted by the cluster, which can be used to produce experimental AFC spectra following the format of Fig. 1. First, one can apply a blind source separation method widely used in the fields of signal processing, acoustics, medical imaging, and neurobiology [65] for extracting a particular component contribution from a set of mixed signals without relying on any information about the mixing process. Second, one can use the experimental approach described and validated in our earlier paper [66]. There, a temporal sequence of images of a vibrating object was recorded using a high-speed camera that was subsequently processed using a Fourier transform-based algorithm yielding information about the oscillation spectrum. This procedure can be applied to a small cluster of oscillating gas bubbles such as those of interest in the current paper, provided that a camera with a sufficiently high frame rate (compared to temporal dynamics of individual gas bubbles in the cluster) is available. This method can be used in conjunction with a bubble pattern recognition technique relying on an artificial neural network algorithm [67], which, in particular, should be applicable when the bubble number in a cluster is large or if bubbles interact in a complex way.

[1] N. Picqué and T. W. Hänsch, Frequency comb spectroscopy, Nat. Photon. **13**, 146 (2019).

[2] T. Fortier and E. Baumann, 20 years of developments in optical frequency comb technology and applications, Comms. Phys. **2**, 153 (2019).

[3] L. S. Cao, D. X. Qi, R. W. Peng, M. Wang, and P. Schmelcher, Phononic Frequency Combs through Nonlinear Resonances, Phys. Rev. Lett. **112**, 075505 (2014).

[4] H. Xiong, L.-G. Si, X.-Y. Lü, and Y. Wu, Optomechanically induced sum sideband generation, Opt. Express **24**, 5773 (2016).

[5] C. Cao, S.-C. Mi, T.-J. Wang, R. Zhang, and C. Wang, Optical high-order sideband comb generation in a photonic molecule optomechanical system, IEEE J. Quantum Electron. **52**, 7000205 (2016).

[6] A. Ganesan, C. Do, and A. Seshia, Phononic Frequency Comb via Intrinsic Three-Wave Mixing, Phys. Rev. Lett. **118**, 033903 (2017).

[7] I. S. Maksymov and A. D. Greentree, Synthesis of discrete phase-coherent optical spectra from nonlinear ultrasound, Opt. Express **25**, 7496 (2017).

[8] E. Garmire, Stimulated Brillouin review: Invented 50 years ago and applied today, Int. J. Opt. **2018**, 2459501 (2018).

[9] H. Wu, Z. Qian, H. Zhang, X. Xu, B. Xue, and J. Zhai, Precise underwater distance measurement by dual acoustic frequency combs, Ann. Phys. (Berlin) **531**, 1900283 (2019).

[10] I. S. Maksymov and A. D. Greentree, Coupling light and sound: Giant nonlinearities from oscillating bubbles and droplets, Nanophotonics **8**, 367 (2019).

[11] M. Goryachev, S. Galliou, and M. E. Tobar, Generation of ultralow power phononic combs, Phys. Rev. Research **2**, 023035 (2020).

[12] J. T. Friedlein, E. Baumann, K. A. Briggman, G. M. Colacion, F. R. Giorgetta, A. M. Goldfain, D. I. Herman, E. V. Hoenig, J. Hwang, N. R. Newbury, E. F. Perez, C. S. Yung, I. Coddington, and K. C. Cossel, Dual-comb photoacoustic spectroscopy, Nat. Commun. **11**, 3152 (2020).

[13] B. Q. H. Nguyen, I. S. Maksymov, and S. A. Suslov, Acoustic frequency combs using gas bubble cluster oscillations in liquids: a proof of concept, Sci. Reps. **11**, 38 (2021).

[14] M. Kumazawa, H. Higashihara, and T. Nagai, Development of acoustic frequency comb technology by ACROSS appropriate for active monitoring of the earthquake field, in *Japan Geoscience Union Meeting* (Japan Geoscience Union, Yokohama, Japan, 2014), Vol. SSS25-02.

[15] I. S. Grudinin, H. Lee, O. Painter, and K. J. Vahala, Phonon Laser Action in a Tunable Two-Level System, Phys. Rev. Lett. **104**, 083901 (2010).

[16] R. P. Beardsley, A. V. Akimov, M. Henini, and A. J. Kent, Coherent Terahertz Sound Amplification and Spectral Line Narrowing in a Stark Ladder Superlattice, Phys. Rev. Lett. **104**, 085501 (2010).

[17] K. Stannigel, P. Komar, S. J. M. Habraken, S. D. Bennett, M. D. Lukin, P. Zoller, and P. Rabl, Optomechanical Quantum Information Processing with Photons and Phonons, Phys. Rev. Lett. **109**, 013603 (2012).

[18] C. E. Brennen, *Cavitation and Bubble Dynamics* (Oxford University Press, New York, 1995).

[19] P. A. Hwang and W. J. Teague, Low-frequency resonant scattering of bubble clouds, J. Atmos. Oceanic Technol. **17**, 847 (2000).

[20] E. S. Nasibullaeva and I. S. Akhatov, Bubble cluster dynamics in an acoustic field, J. Acoust. Soc. Am. **133**, 3727 (2013).

[21] M. Minnaert, On musical air-bubbles and the sound of running water, Phil. Mag. **16**, 235 (1933).

[22] M. Zhang, B. Buscaino, C. Wang, A. Shams-Ansari, C. Reimer, R. Zhu, J. M. Kahn, and M. Lončar, Broadband electro-optic frequency comb generation in a lithium niobate microring resonator, Nature (London) **568**, 373 (2019).

[23] Y. A. Kobelev, L. A. Ostrovskii, and A. M. Sutin, Self-illumination effect for acoustic waves in a liquid with gas bubbles, Zh. Eksp. Teor. Fiz. **30**, 423 (1979).

[24] P. L. Marston, E. H. Trinh, J. Depew, and J. Asaki, Response of bubbles to ultrasonic radiation pressure: Dynamics in low gravity and shape oscillations, in *Bubble Dynamics and Interface Phenomena*, edited by J. R. Blake, J. M. Boulton-Stone, and N. H. Thomas (Kluwer Academic, Dordrecht, 1994), pp. 343–353.

[25] A. A. Doinikov and S. T. Zavtrak, On the "bubble grapes" induced by a sound field, J. Acoust. Soc. Am. **99**, 3849 (1996).

[26] D. Rabaud, P. Thibault, M. Mathieu, and P. Marmottant, Acoustically Bound Microfluidic Bubble Crystals, Phys. Rev. Lett. **106**, 134501 (2011).

[27] A. E. Zabolotskaya, Interaction of gas bubbles in a sound field, Sov. Phys. Acoust. **30**, 365 (1984).

[28] J. B. Keller and M. Miksis, Bubble oscillations of large amplitude, J. Acoust. Soc. Am. **68**, 628 (1980).

[29] L. Rayleigh, On the pressure developed in a liquid during the collapse of a spherical cavity, Phyl. Mag. **34**, 94 (1917).

[30] M. S. Plesset, The dynamics of cavitation bubbles, J. Appl. Mech. **16**, 228 (1949).

[31] R. Mettin, I. Akhatov, U. Parlitz, C. D. Ohl, and W. Lauterborn, Bjerknes forces between small cavitation bubbles in a strong acoustic field, Phys. Rev. E **56**, 2924 (1997).

[32] F. Dzaharudin, S. A. Suslov, R. Manasseh, and A. Ooi, Effects of coupling, bubble size, and spatial arrangement on chaotic dynamics of microbubble cluster in ultrasonic fields, J. Acoust. Soc. Am. **134**, 3425 (2013).

[33] D. Fuster and T. Colonius, Modelling bubble clusters in compressible liquids, J. Fluid Mech. **688**, 352 (2011).

[34] B. E. Nemtsov, Effects of the radiation interaction of bubbles in a fluid, Pis'ma Zh. Tekh. Fiz. **9**, 858 (1983).

[35] T. Watanabe and Y. Kukita, Translational and radial motions of a bubble in an acoustic standing wave field, Phys. Fluids A **5**, 2682 (1993).

[36] N. A. Pelekasis and J. A. Tsamopoulos, Bjerknes forces between two bubbles. Part 2. Response to an oscillatory pressure field, J. Fluid Mech. **254**, 501 (1993).

[37] A. A. Doinikov and S. T. Zavtrak, On the mutual interaction of two gas bubbles in a sound field, Phys. Fluids **7**, 1923 (1995).

[38] T. Barbat, N. Ashgriz, and C.-S. Liu, Dynamics of two interacting bubbles in an acoustic field, J. Fluid Mech. **389**, 137 (1999).

[39] A. Harkin, T. J. Kaper, and A. Nadim, Coupled pulsation and translation of two gas bubbles in a liquid, J. Fluid Mech. **445**, 377 (2001).

[40] A. A. Doinikov, Translational motion of two interacting bubbles in a strong acoustic field, Phys. Rev. E **64**, 026301 (2001).

[41] Y. Matsumoto and S. Yoshizawa, Behavior of a bubble cluster in an ultrasound field, Int. J. Numer. Methods Fluids **47**, 6 (2005).

[42] C. A. Macdonald and J. Gomatam, Chaotic dynamics of microbubbles in ultrasonic fields, Proc. Inst. Mech. Eng., Part C: J. Mech. Eng. Sci. **220**, 333 (2006).

[43] R. Mettin and A. A. Doinikov, Translational instability of a spherical bubble in a standing ultrasound wave, Appl. Acoust. **70**, 1330 (2009).

[44] K. Yasui, T. Tuziuti, J. Lee, T. Kozuka, A. Towata, and Y. Iida, Numerical simulations of acoustic cavitation noise with the temporal fluctuation in the number of bubbles, Ultrason. Sonochem. **17**, 460 (2010).

[45] R. Sadighi-Bonabi, N. Rezaee, H. Ebrahimi, and M. Mirheydari, Interaction of two oscillating sonoluminescence bubbles in sulfuric acid, Phys. Rev. E **82**, 016316 (2010).

[46] L. Jiang, F. Liu, H. Chen, J. Wang, and D. Chen, Frequency spectrum of the noise emitted by two interacting cavitation bubbles in strong acoustic fields, Phys. Rev. E **85**, 036312 (2012).

[47] M. Lanoy, C. Derec, A. Tourin, and V. Leroy, Manipulating bubbles with secondary Bjerknes forces, Appl. Phys. Lett. **107**, 214101 (2015).

[48] G. S. B. Lebon, K. Pericleous, I. Tzanakis, and D. G. Eskin, Dynamics of two interacting hydrogen bubbles in liquid aluminum under the influence of a strong acoustic field, Phys. Rev. E **92**, 043004 (2015).

[49] A. A. Doinikov, *Bubble and Particle Dynamics in Acoustic Fields: Modern Trends and Applications* (Research Signpost, Kerala, India, 2005).

[50] V. Bjerknes, *Fields of Force* (The Columbia University Press, New York, 1906).

[51] T. G. Leighton, A. J. Walton, and M. J. W. Pickworth, Primary Bjerknes forces, Eur. J. Phys. **11**, 47 (1990).

[52] G. N. Kazantsev, The motion of gaseous bubbles in a liquid under the influence of Bjerknes forces arising in an acoustic field, Sov. Phys. Dokl. **4**, 1250 (1960).

[53] L. A. Crum, Bjerknes forces on bubbles in a stationary sound field, J. Acoust. Soc. Am. **57**, 1363 (1975).

[54] I. Akhatov, U. Parlitz, and W. Lauterborn, Towards a theory of self-organization phenomena in bubble-liquid mixtures, Phys. Rev. E **54**, 4990 (1996).

[55] N. A. Pelekasis, A. Gaki, A. A. Doinikov, and J. A. Tsamopuolos, Secondary Bjerknes forces between two bubbles and the phenomenon of acoustic streamers, J. Fluid Mech. **500**, 313 (2004).

[56] H. N. Oguz and A. Prosperetti, A generalization of the impulse and virial theorems with an application to bubble oscillations, J. Fluid Mech. **218**, 143 (1990).

[57] M. Ida, Alternative interpretation of the sign reversal of secondary Bjerknes force acting between two pulsating gas bubbles, Phys. Rev. E **67**, 056617 (2003).

[58] S. A. Suslov, A. Ooi, and R. Manasseh, Nonlinear dynamic behavior of microscopic bubbles near a rigid wall, Phys. Rev. E **85**, 066309 (2012).

[59] S. H. Chen, J. L. Huang, and K. Y. Sze, Multidimensional Lindstedt-Poincaré method for nonlinear vibration of axially moving beams, J. Sound Vib. **306**, 1 (2007).

[60] R. Manasseh and A. Ooi, Frequencies of acoustically interacting bubbles, Bubble Sci. Eng. Technol. **1**, 58 (2016).

[61] A. A. Doinikov, Mathematical model for collective bubble dynamics in strong ultrasound fields, J. Acoust. Soc. Am. **116**, 821 (2004).

[62] V. G. Levich, *Physicochemical Hydrodynamics* (Prentice-Hall, Englewood Cliffs, NJ, 1962).

[63] V. G. Levich, The motion of bubbles at high Reynolds numbers, Zh. Eksp. Teor. Fiz. **18**, 49 (1949).

[64] A. E. Mudrov, *Numerical Methods for Personal Computers in Basic, Fortran, and Pascal* (in Russian) (Rasko, Tomsk, 1990).

[65] P. Comon and C. Jutten, *Handbook of Blind Source Separation: Independent Component Analysis and Applications* (Academic Press, Cambridge, 2010).

[66] I. S. Maksymov and A. Pototsky, Excitation of Faraday-like body waves in vibrated living earthworms, Sci. Reps. **10**, 8564 (2020).

[67] I. Poletaev, M. P. Tokarev, and K. S. Pervunin, Bubble patterns recognition using neural networks: Application to the analysis of a two-phase bubbly jet, Int. J. Multiph. Flow **126**, 103194 (2020).